Crystal structure and magnetic ordering of Mn and Ce in La$_{0.7}$Ce$_{0.15}$Ca$_{0.15}$MnO$_3$

Crystal structure and magnetic ordering of Mn and Ce in $La_{0.7}Ce_{0.15}Ca_{0.15}MnO_3$

S Y Wu[1], C C Yang[1], F C Tsao[1], W-H Li[1], K C Lee[1], J W Lynn[2] and H D Yang[3]

[1] Department of Physics, National Central University, Chung-Li 32054, Taiwan
[2] NIST Center for Neutron Research, NIST, Gaithersburg, MD 20899-8562, USA
[3] Department of Physics, National Sun Yat-Sen University, Kaohsiung 80424, Taiwan

Abstract
Neutron diffraction, ac magnetic susceptibility and magnetization measurements have been performed to study the magnetic properties of Ce-doped $La_{0.7}Ce_{0.15}Ca_{0.15}MnO_3$. A slightly distorted monoclinic $P2_1/c$ symmetry for the crystal structure was found to describe the high-resolution powder diffraction pattern, taken at room temperature, better than the normally used orthorhombic *Pnma* symmetry does. Three anomalies, at around 165, 105 and 38 K, were clearly evident in the ac susceptibility measurements. Neutron diffraction measurements then confirmed that the anomaly at high temperature is associated with the ferromagnetic ordering of the Mn spins, whereas the low-temperature one corresponds to the ordering of the Ce spins. The ordering temperatures for the Mn and Ce spins were found to be at T_C(Mn) 180 K and T_C(Ce) 45 K, respectively, with a saturated moment of $\langle \mu_z \rangle = 2.54(5)$ μ_B for the Mn spins and an average moment of 0.27(3) μ_B on the rare-earth sites.

(Some figures in this article are in colour only in the electronic version)

1. Introduction

The strong interplay between the structure, magnetism and electronic transport has generated a large variety of interesting properties [1–6] in the hole-doped perovskite-type manganese oxides. It has been realized that the creation of a mixed-valent state, where both Mn^{3+} and Mn^{4+} ions are present, is essential for the double-exchange (DE) interaction [7, 8] to operate and gives rise to colossal magnetoresistance (CMR) [9–11] and related phenomena. Depending on the doping concentration, these systems exhibit quite different magnetic and transport behaviours. In many cases, the tilting distortion of the MnO_6 octahedral framework, resulting from smaller cations being used for doping, is superimposed on the imperfection of the octahedron, caused by the Jahn–Teller effect, which leads to the complicated magnetic and electric properties for the systems. Generally speaking, the hole carrier density and the overlapping between the

manganese and the oxygen orbitals are the two key parameters that govern the transport and magnetic properties of the systems. In $La_{1-x}Ca_xMnO_3$ (La113) the maximum CMR effect occurs at $x = 1/3$ [12], where ferromagnetic couplings among the Mn ions have been found. It is known that the ionic radius of Ce is considerably smaller than that of La. Modifications in the MnO_6 octahedron, and hence the strength of DE interactions, may be expected, when Ce ions are used to replace the La ions. Ce doping causes the O atoms in both the LaO and the MnO_2 layers to shift further away from the centre positions, so that smaller Mn–O–Mn angles and a larger apical distortion in the MnO_6 octahedron result. The substitution also leads to increases in all three unit-cell parameters, and hence the unit-cell volume, but a reduced degree of orthorhombicity of the basal MnO_2 plane [13]. Ce-doped $RMnO_3$ (R = rare earth) manganites have recently been investigated [13–17], and the CMR effect was observed and is sensitive to the stoichiometry. In this paper, we report results of studies made on the structural and magnetic properties of polycrystalline $La_{0.7}Ce_{0.15}Ca_{0.15}MnO_3$. A slightly distorted monoclinic $P2_1/c$ symmetry for the crystal structure was found to describe the high-resolution powder pattern, taken at room temperature, better than the orthorhombic *Pnma* symmetry does. In addition, a long-range ferromagnetic ordering of the Mn spins, with T_C(Mn) 180 K, and an induced ordering of the Ce spins, with T_C(Ce) 45 K, were observed.

2. Crystal structure

A polycrystalline sample of nominal composition $La_{0.7}Ce_{0.15}Ca_{0.15}MnO_3$ was prepared employing the standard solid-state reaction technique. A stoichiometric mixture of high-purity La_2O_3, CeO_2, $CaCO_3$ and Mn_2O_3 powders was ground and heated at 1100 °C for 24 h. The resultant powder was then pressed into small pellets and sintered at 1250 °C for 24 h and then at 1350 °C for another 24 h. After regrinding and repressing, the pellets were sintered again at 1400 °C for 24 h. X-ray diffraction was used to first characterize the sample, pellet by pellet. No obvious differences were found in the x-ray diffraction patterns taken from different portions of the sample. High-resolution neutron powder diffraction was then employed to determine the detailed crystalline structure. The measurements were performed at the NIST Center for Neutron Research and the data were collected on BT-1, the 32-detector powder diffractometer, using a Cu(311) monochromator crystal to extract neutrons of wavelength 1.5401 Å. Angular collimators, with horizontal divergences of 15′, 20′ and 7′ full width at half maximum (FWHM) acceptance, were employed for the in-pile, monochromatic and diffracted beams, respectively. During the measurement the sample was loaded into a cylindrical vanadium can, which gave rise to no measurable neutron diffraction peaks. Many studies [4, 11, 18] have concluded that the Ca-doped La113 compounds have an orthorhombic *Pnma* symmetry in the crossover region at room temperature. Breakdown of the orthorhombic symmetry on a micro-domain scale has been reported [19, 20]. A phase separation into two structural phases that contain the parent orthorhombic structure together with a slightly distorted monoclinic structure has also been observed [21, 22]. Recently, a structural study [23] combining electron diffraction, electron microscopy and neutron powder diffraction revealed a monoclinic $P2_1/c$ structure for a 15% Ca-doped La113 compound at room temperature, with an orthorhombic *Pnma* symmetry at low temperatures. A structural transition from an orthorhombic *Imma* symmetry to a tetragonal $I4/mcm$ symmetry has also been identified [17] in a 40% Ce-doped Pr113 compound. All these observations indicate that the detailed crystal symmetry of the 113 compounds is quite sensitive to chemical composition. In our structural analysis we then pay special attention to searching for the possible symmetries that can describe the observed diffraction pattern well. The diffraction patterns were analysed using the General Structure Analysis System (GSAS) program [24], following the Rietveld refinement method [25]. Several models with different
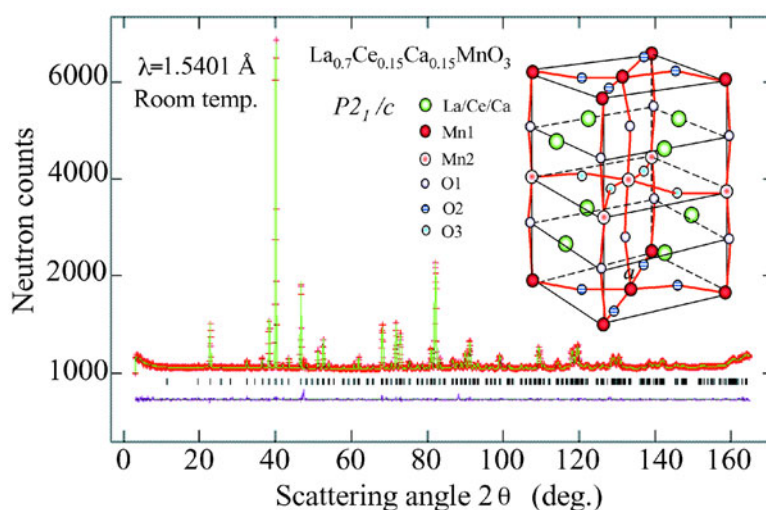
Figure 1. Observed (crosses) and fit (solid curves) diffraction patterns, assuming a monoclinic $P2_1/c$ symmetry, taken at room temperature. The vertical lines shown below the pattern mark the angular positions of the calculated Bragg reflections. Shown at the bottom are the differences between the observed and the calculated patterns.

symmetries were assumed during the preliminary analysis. All the structural and lattice parameters were allowed to vary simultaneously, and refining processes were carried out until R_w, the weighted R factor, differed by less than one part in a thousand within two successive cycles. Two types of crystal structure, one belonging to the monoclinic $P2_1/c$ symmetry and the other to the orthorhombic *Pnma* symmetry, were found to fit the diffraction pattern well. However, the $P2_1/c$ structure ($R_p = 5.17\%$, $R_w = 7.20\%$, $\chi^2 = 1.464$) fits slightly better than the *Pnma* one ($R_p = 5.21\%$, $R_w = 7.27\%$, $\chi^2 = 1.498$). Figure 1 shows the observed (crosses), fitted (solid lines) and difference patterns using a model with a monoclinic $P2_1/c$ symmetry. The portions of the diffraction pattern around the characteristic {220} + {022} and {440} + {044} peaks for the two structures are plotted together in figure 2 for a direct comparison, and indicate that the fit using $P2_1/c$ symmetry is evidently better than the one using *Pnma*, as can be seen from the difference patterns plotted at the bottom of each plot. This result is similar to what was reported [23] for a $La_{0.85}Ca_{0.15}MnO_3$ sample. Table 1 summarizes the refined structural parameters of the two models. Note that the monoclinic $P2_1/c$ structure can be viewed as a slightly distorted ($\theta = 90.109°$) orthorhombic *Pnma* structure, so that nonequivalent MnO_6 octahedra are obtained. Careful analysis of the occupancy factors shows that all sites are almost fully occupied. Both the $P2_1/c$ and the *Pnma* fits give a chemical composition of $La_{0.7}Ce_{0.51}Ca_{0.49}MnO_{2.99}$ for the compound, which agrees very well with the stoichiometric composition. In addition, the structural analysis was also used to search for impurity phases, especially MnO_2, but no additional peaks were present, indicating that the sample is single phase. We estimate that any impurity phase is less than 1%.

3. Magnetic response

AC magnetic susceptibility and dc magnetization measurements, using conventional setups, were performed to search for magnetic responses. For the ac susceptibility, both the in-phase component χ' and the out-of-phase component χ'' were measured, covering 1.4–300 K. These
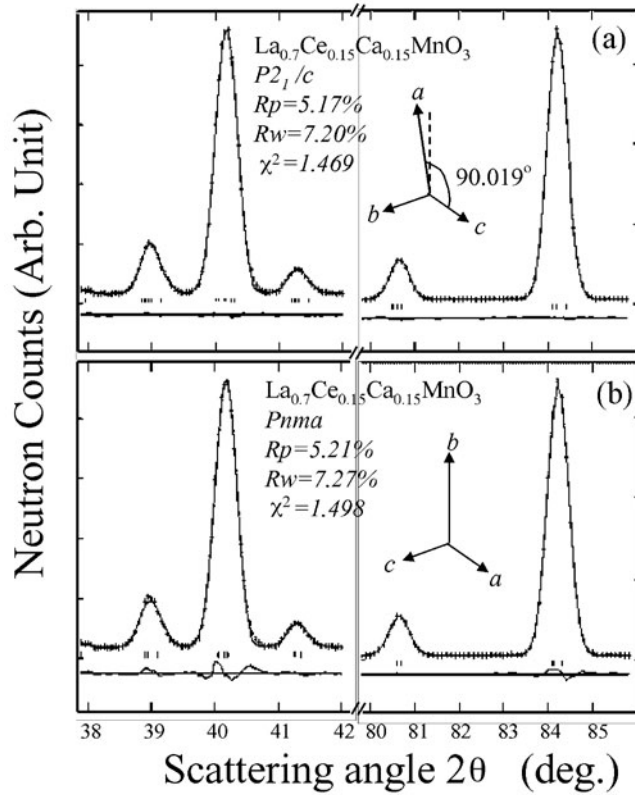
Figure 2. The characteristic {022} +{220} and {044} + {440} peaks for the two proposed structures are plotted together, using an expanded scale to facilitate a direct comparison. The fit using a monoclinic $P2_1/c$ symmetry is slightly better than that using an orthorhombic *Pnma* symmetry, as can be seen from the difference patterns plotted at the bottom and the goodness parameters in the insets.

data were collected by employing weak driving fields with various strengths and frequencies, with and without the presence of an applied dc magnetic field. We note that χ' measures the response of the system to the driving field, whereas χ'' signifies the dissipative loss of the driving field to the system. Figure 3(a) shows the variations of χ' and χ'' with temperature, measured using a driving field with an rms strength of 1 Oe and a frequency of 100 Hz. The main features seen in $\chi'(T)$ (filled circles) are the peak marked T_{m1} at 165 K (peak position), the anomaly marked T_S at 105 K (inflection point) and the anomaly marked T_{m2} at 38 K (inflection point). Each anomaly in $\chi'(T)$ is associated with a dissipative loss, as seen in $\chi'(T)$ (open circles), where two peaks and an anomaly are clearly evident. No obvious differences were found for $\chi'(T)$ and $\chi''(T)$ measured using a higher frequency for the driving field (up to 104 Hz), indicating that the relaxation rates of the associated responses are much higher than the frequency used. No spin-glass behaviour was observed for the present Ce-doped compound, as stronger responses in χ' and χ'' were obtained for the measurements made using a stronger driving field, opposite to what would be expected for a spin glass system. This observation is different from what has been reported [16] for a Tb-doped system, where spin-glass behaviour was suggested. An applied dc magnetic field, on the other hand, suppresses the amplitudes and alters the profiles of χ' and χ'' significantly, as seen in figure 3(b), where $\chi'(T)$ and

Table 1. Refined structural parameters of La$_{0.7}$Ce$_{0.153}$Ca$_{0.147}$MnO$_{2.99}$ at room temperature, assuming the monoclinic $P2_1/c$ and orthorhombic *Pnma* symmetries. B (Å^2) represents the isotropic temperature parameter.

Space group $P21/c$, $a = 7.7655(2)$ Å, $b = 5.5062(1)$ Å, $c = 5.4883(1)$ Å
$\alpha = 90°$, $\beta = 90.109(3)°$, $\gamma = 90°$

Atom		X	Y	Z	B (Å^2)	Occupancy
La	4e	0.2508(6)	−0.0040(5)	−0.0212(3)	0.80(3)	0.7
Ce	4e	0.2508(6)	−0.0040(5)	−0.0212(3)	0.80(3)	0.153(3)
Ca	4e	0.2508(6)	−0.0040(5)	−0.0212(3)	0.80(3)	0.147(2)
O(1)	4e	0.2495(1)	0.0655(5)	0.5088(5)	1.01(6)	0.997(2)
Mn(1)	2c	0	1	0.5	0.29(1)	1
O(2)	4e	0.0338(6)	0.7301(9)	0.7223(9)	0.88(4)	1.003(3)
Mn(2)	2d	0	0	0.5	0.38(1)	1
O(3)	4e	0.4640(6)	−0.2176(1)	0.2224(1)	1.24(1)	0.999(3)

$R_p(\%) = 5.17$ $R_w(\%) = 7.20$ $\chi^2 = 1.464$

Space group *Pnma*, $a = 5.4882(1)$ Å, $b = 7.7683(2)$ Å, $c = 5.5062(1)$ Å
$\alpha = 90°$, $\beta = 90°$, $\gamma = 90°$

Atom		X	Y	Z	B (Å^2)	Occupancy
La	4c	0.0212(3)	0.25	0.4963(5)	0.84(2)	0.7
Ce	4c	0.0212(3)	0.25	0.4963(5)	0.84(2)	0.153(2)
Ca	4c	0.0212(3)	0.25	0.4963(5)	0.84(2)	0.147(2)
O(1)	4c	0.4913(5)	0.25	0.5657(4)	1.05(6)	0.997 (3)
Mn	4b	0	0	0	0.34(3)	1
O(2)	8d	0.2772(3)	0.0349(2)	0.2238(3)	1.08(4)	1.001(5)

$R_p(\%) = 5.21$ $R_w(\%) = 7.27$ $\chi^2 = 1.498$

$\chi''(T)$, measured with various applied fields for H_{dc}, are plotted. It appears that the responses are strongly suppressed by the applied field. The peak at T_{m1} is associated with the ordering of the Mn spins (see below). A ferromagnetic character was observed for this peak, as the peak position shifts to a much higher temperature when H_{dc} is applied. Figure 4(a) shows the variation of T_{m1} with H_{dc}, revealing that T_{m1} shifts from 165 K at $H_{dc} = 0$ to 242 K at $H_{dc} = 9$ T, a 50% increase, while the rate of increase for T_{m1} is reduced at high H_{dc}. This increase in T_{m1} is consistent with the ferromagnetic DE being enhanced by the applied field, as has been observed [11] in many CMR compounds. However, the amount of increase observed for the present Ce-doped compound is substantially higher than that for other related systems. Magnetic hysteresis was also observed at temperatures below T_{m1}, as shown in figure 5, where the magnetization as a function of H_{dc}, taken at four representative temperatures, is plotted. A weak but definitive magnetic hysteresis begins to appear at 160 K; and becomes more pronounced as the temperature is further reduced. The anomaly marked by T_S also appeared in the Ce-free compounds, indicating that the appearance of Ce may not be the main origin of this anomaly. In La$_{0.85}$Ca$_{0.15}$MnO$_3$, it has been attributed [23] to the structural change from a monoclinic $P2_1/c$ symmetry at high temperatures to an orthorhombic *Pnma* symmetry at low temperatures. Our neutron magnetic diffraction measurements show no obvious magnetic signals to be associated with this anomaly. In addition, the anomaly is completely smeared by an applied field of 0.3 T, as seen in figure 3(b), suggesting that the application of a magnetic field enhances the ferromagnetic exchange but weakens the environment for the onset of the structural change and suppresses the anomaly linked to it. The anomaly marked by T_{m2} is
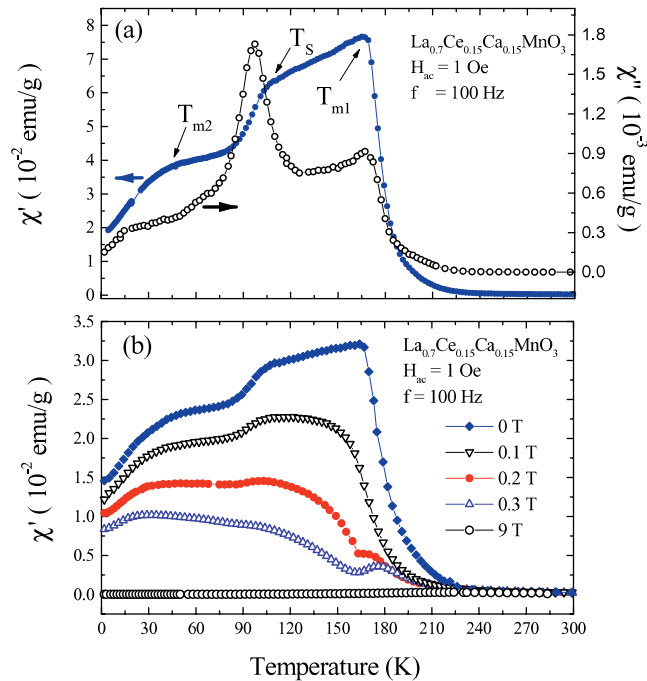
Figure 3. (a) Temperature dependences of χ' and χ'', measured using a weak driving field with an rms strength of 1 Oe and a frequency of 100 Hz. Three anomalies marked as T_{m1}, T_S and T_{m2} are clearly evident. (b) Effect of applied field on $\chi'(T)$. H_{dc} significantly alters $\chi'(T)$, with T_{m1}, T_S and T_{m2} affected differently.

a direct result of Ce doping, since it does not appear in Ce-free systems, and signifies the ordering of the Ce spins. It shifts rapidly to lower temperatures with applied fields, indicating antiferromagnetic coupling. Figure 4(b) shows the variation of T_{m2} with H_{dc}, revealing that T_{m2} is reduced from 38 K at $H_{dc} = 0$ to 5 K at 1 T. The temperature dependence of the magnetization, measured using a warming process with a field $H_{dc} = 0.1$ T, is plotted in figure 6. It shows a rapid increase with reducing temperature starting at around 180 K, and the magnetization saturates at around 100 K, indicating the occurrence of a ferromagnetic transition. This is associated with the ordering of the Mn spins. Below 70 K, a sizeable decrease in the magnetization with reducing temperature was seen. However, finite values for the magnetization were obtained at low temperatures, showing that the magnetization decreases when the Ce spins order.

4. Magnetic ordering

Neutron magnetic diffraction patterns, covering certain temperature regimes where the susceptibility shows anomalies, were collected to search for magnetic signals. These measurements were also conducted at the NIST Center for Neutron Research, using the BT-9 triple-axis spectrometer and a pyrolytic graphite PG(002) monochromator crystal to extract =2.359 Å neutrons, and a PG filter to suppress higher-order wavelength contamination. Angular collimations with horizontal divergences of 40′, 48′ and 48′ FWHM acceptance were used for the in-pile, monochromatic and diffracted beams, respectively. A pumped ^{4}He cryostat was used to cool the sample. Diffraction patterns covering the angular range
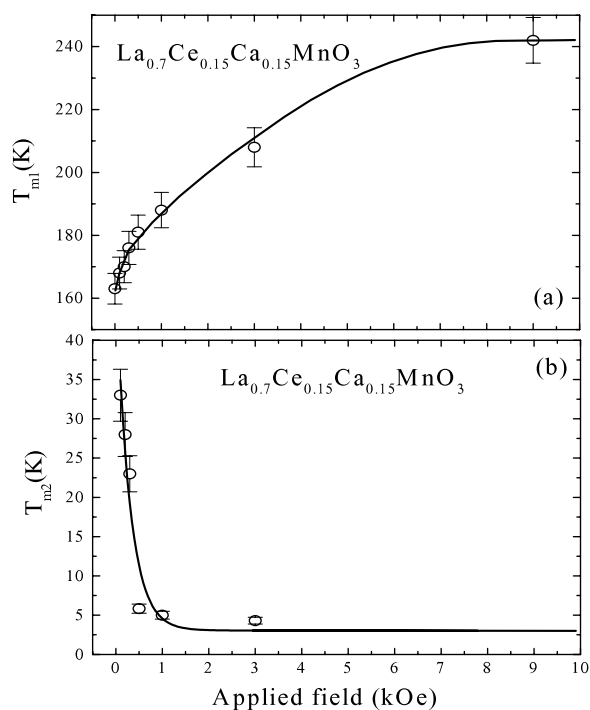
Figure 4. Plot of the variations of T_{m1} and T_{m2} with an applied field. T_{m1} shifts to a higher temperature, whereas T_{m2} shifts to a lower temperature in the presence of an applied field. The solid lines shown are guides to the eye only.

Table 2. The lattice constants obtained at low temperatures.

| Temperature (K) | Space group *Pnma* | | |
	a (Å)	b (Å)	c (Å)
14	5.4611(9)	7.7441(9)	5.4722(8)
50	5.4686(8)	7.7500(8)	5.4885(7)
220	5.4725(6)	7.7604(9)	5.4975(5)

from $2\theta = 5°$ to $65°$ were collected at several temperatures. No significant structural changes were observed over the temperature range studied. Portions of the diffraction patterns taken at three representative temperatures are plotted in figure 7, where the indices shown are based on the low-temperature nuclear orthorhombic *Pnma* unit cell. Only nuclear peaks were seen for the pattern taken at 220 K. Reducing the temperature to 50 K, the intensities of both reflections shown in figure 7 increase significantly. Further reducing the temperature to 14 K, a relatively weak peak at $2\theta = 27.8°$ develops, as seen in the inset to figure 7, while the intensities for the two reflections continue to increase but at a much reduced rate. Two separate magnetic orderings are hence observed, which we associate separately with the Mn and Ce spin orderings. The lattice constants that we obtained at low temperatures are listed in table 2.

4.1. Mn spin ordering

The magnetic diffraction pattern obtained at 50 K is shown in figure 8, where the diffraction pattern taken at 220 K, serving as the non-magnetic background, has been subtracted from
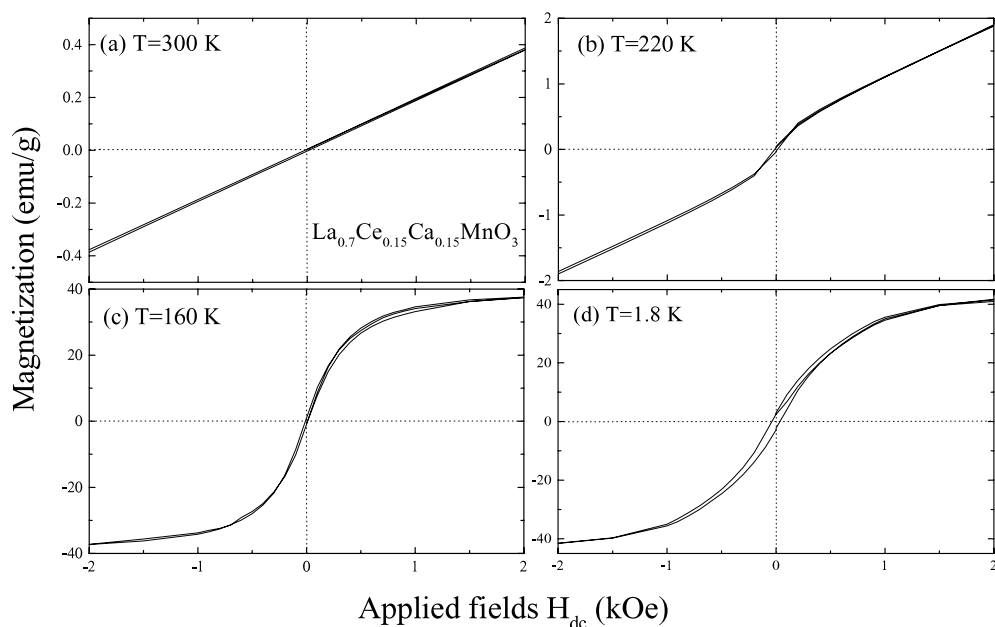
Figure 5. Magnetization curves measured at four representative temperatures. A small but definite magnetic hysteresis develops below 160 K.
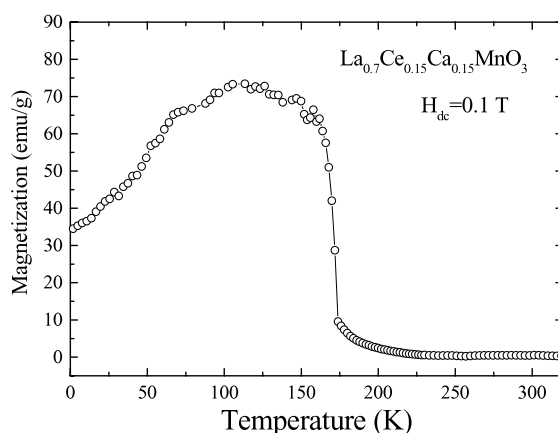

Figure 6. Temperature dependence of the magnetization, measured in a field $H_{dc} = 0.1$ T. A rapid increase starting near 180 K and a decrease below 70 K with reducing temperature are seen.

the data at 50 K. These two resolution-limited peaks signify the long-range ordering of the Mn spins. They appear at the same scattering angles as the nuclear ones do, indicating a ferromagnetic arrangement of the ordered Mn moments. A ferromagnetic arrangement, where the moments point in a direction that is 45° away from the *b*-axis direction, as is shown in the inset to figure 8, fits the observed pattern well. Unfortunately, the specific moment direction in the *a–c* plane cannot be determined from our powder data due to the similarity between the *a* and *c* axes. The solid curves shown in figure 8 indicate the fit using the proposed spin arrangement convoluted with the Gaussian instrumental resolution function, and the overall fit
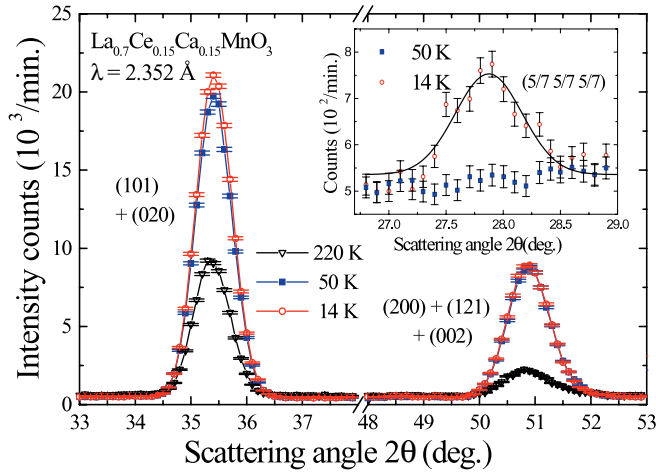
Figure 7. Diffraction patterns observed at three representative temperatures. The indices shown are based on the orthorhombic *Pnma* nuclear unit cell. The solid curves show fits of the data to the Gaussian instrumental resolution function.

is very good. We note however that the moment direction proposed for the Mn ions can only be considered as tentative, since only two magnetic peaks were observed. The temperature dependence of the representative {101} + {020} peak intensity is shown in figure 9. In the temperature regime studied, the background intensity and the widths of the magnetic peaks remain essentially unchanged. The temperature dependence of the peak intensity is then the same as that of the integrated intensity, representing the variation of the square of the order parameter with temperature. The ordering temperature of the Mn spins, as determined by the inflection point of the order parameter curve, is T_C(Mn) 180 K. The Mn spin ordering gives rise to the most pronounced anomaly in $\chi'(T)$, shown in figure 3(a), where the transition is marked as T_{m1}. This T_C for the present 15% Ce-doped compound is much lower than the 233 K observed [14, 16] for the 30% Ce-doped compound. On reducing the temperature the intensity increases monotonically. Around 50 K, a plateau is evident as shown in the inset to figure 9, indicating that the Mn moments have saturated, while below 50 K the peak at $2\theta = 27.8°$ begins to develop. By comparing the magnetic intensities obtained at 50 K with the nuclear ones, we obtain a saturated moment of $\langle \mu_z \rangle = 2.54(5)$ μ_B for the Mn spins, which is about 10% smaller than what is usually obtained [18, 23] in Ce-free La$_{0.85}$Ca$_{0.15}$MnO$_3$. This, we believe, is a direct result of the crystal field effect on the Mn 3d moments.

4.2. Ce spin ordering

Figure 10 shows the change in the magnetic diffraction pattern as the temperature is reduced from 50 to 14 K. The main new feature is the development of the resolution-limited reflection at $2\theta = 27.8°$, which is accompanied by further increases in the {101} + {020} and {200} + {121} + {002} intensities. If the increases in the {101} + {020} and {200} + {121} + {002} intensities are due to further increases in the Mn moments, an intensity ratio of $R \equiv I_{\{101\}+\{020\}}/I_{\{200\}+\{121\}+\{002\}} = 1.5$ is then expected, which differs significantly from the observed value of $R = 8.4$. Developments of moments on the other sites may then be anticipated. In addition, the reflection at $2\theta = 27.8°$ cannot be indexed using simple Miller indices, if based on the nuclear unit cell. It, however, fits to the {555} reflection of the Ce
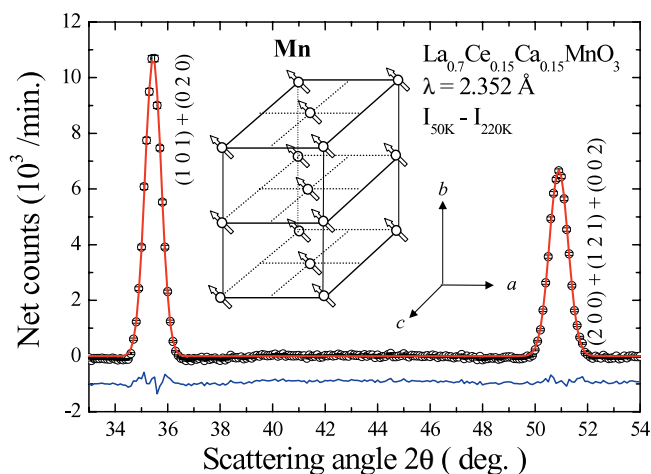
Figure 8. Magnetic diffraction pattern observed at 50 K. The inset plots the magnetic structure of the Mn spins that fits the observed pattern. The solid curves are the fitted pattern, using the proposed model convoluted with the instrumental resolution.
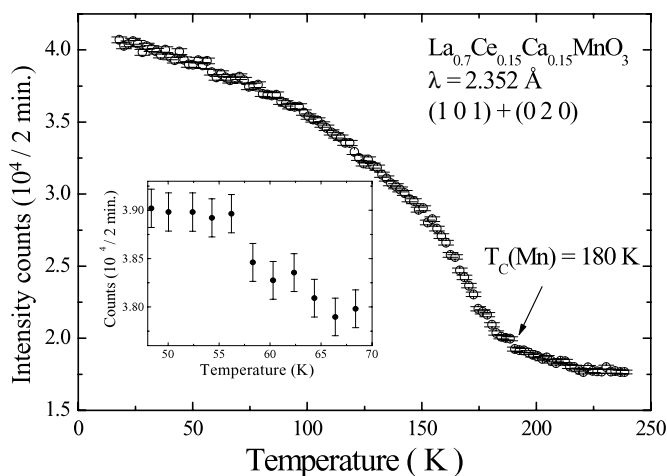

Figure 9. Temperature dependence of the {101} + {020} peak intensity, showing a T_C(Mn) of 180 K for the Mn spins. A plateau appears at around 50 K as seen in the inset, indicating that the Mn moments saturate around 50 K.

unit cell, which is seven times the nuclear one along all three crystallographic directions. Based on the nuclear unit cell, this reflection may then be indexed as the {5/7 5/7 5/7} reflection. Most likely, the magnetic peaks shown in figure 10 are associated with the ordering of the Ce spins. The contributions of the ordered Ce moments to the {101} + {020} and {200} + {121} + {002} reflections preclude an antiferromagnetic configuration for the Ce spins, while the susceptibility data shown in figure 3(b) indicate that an applied field shifts the transition to a lower temperature. Accordingly, we conclude that the Ce moments point in the same direction, but opposite to the ferromagnetic Mn moments, as shown in the inset to figure 11. Figure 11 shows the observed (open circles) and calculated (solid curves) magnetic diffraction patterns at 14 K. In the calculation, the Mn moments were taken to be at 2.54 μ_B
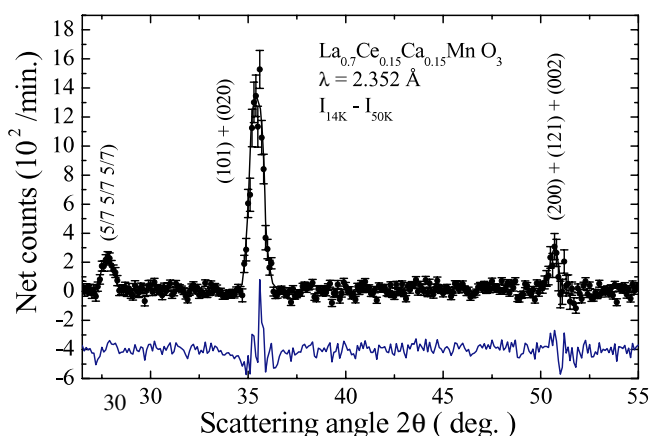
Figure 10. Magnetic peaks develop as the temperature is reduced from 50 to 14 K. The solid curves are fits of the data to the Gaussian instrumental resolution function.
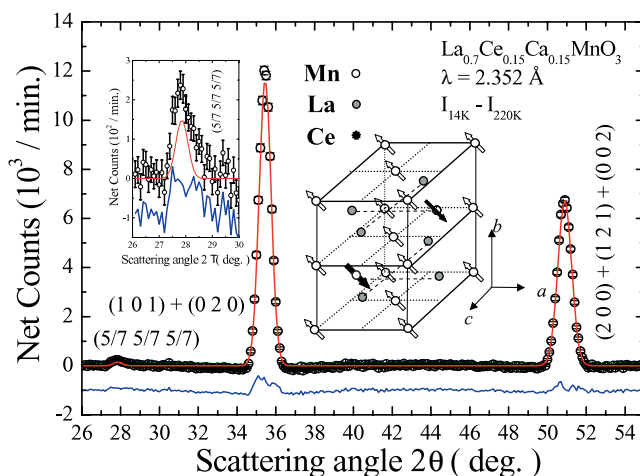

Figure 11. Magnetic diffraction pattern observed at 14 K. The inset plots the magnetic structure that fits the observed pattern. The solid curves are the calculated pattern, using the proposed model convoluted with the instrumental resolution. The calculated (solid curve) and observed (open circles) intensities of the {5/7 5/7 5/7} reflection are also plotted in the inset, using expanded scales.

(as they have saturated at 50 K) and the unit cell was taken to be seven times the one shown in the inset along all three crystallographic directions, assuming the Ce ions occupied the same site in each sub-cell. Calculations assuming the Ce ions occupied other rare-earth sizes give essentially the same results. The fit is reasonably good. The average moment on the rare-earth site is 0.27(3) μ_B, which corresponds to a moment of 1.89 μ_B on each Ce ion, assuming that the Ce ions are randomly distributed on the rare-earth sites. The proposed antiferromagnetic coupling between the Mn and Ce ions in the present compound agrees with that suggested for a 40% Ce-doped Pr$_{0.1}$Ce$_{0.4}$Sr$_{0.5}$MnO$_3$ [17]. However, work on single-crystal samples, where more magnetic reflections may be identified, will be needed to elucidate the detailed arrangement for the Ce spins. The variation of the {5/7 5/7 5/7} peak intensity with temperature is shown in figures 12(a) and (b) shows the low-temperature portion of the
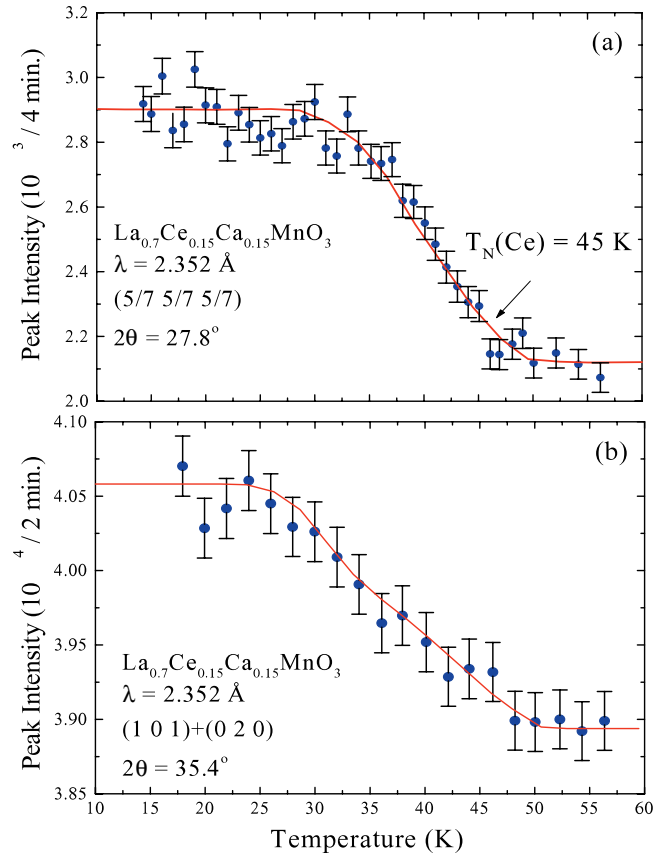
Figure 12. Temperature dependences of the (a) {5/7 5/7 5/7} and (b) {101} +{020} peak intensities, where the solid curves shown are guides to the eye only. Both plots reveal a T_C(Ce) 45 K for the Ce spins.

{101} + {020} order parameter curve using an expanded scale. Both curves show an ordering temperature of T_C(Ce) 45 K for the Ce spins. Correspondingly, an anomaly, marked as T_{m2}, is also seen in $\chi'(T)$ (see figure 3(a)). We believe that the separation between the nearest Ce ions in the present 15% Ce-doped compound is too large to develop coupling without being assisted by neighbouring Mn ions. The relatively high ordering temperature observed for the Ce spins, together with the observation that it is strongly affected by an applied magnetic field, indicate that the ordering of the well separated Ce moments is induced by the ferromagnetic Mn moments.

5. Conclusions

We have studied the crystal structure and magnetic properties of a polycrystalline $La_{0.7}(Ce_{0.51}Ca_{0.49})_{0.3}MnO_{2.99}$ sample, fabricated using the standard solid-state reaction techniques. Three transitions were observed to be associated with structural change, Mn spin ordering and induced Ce spin ordering. At room temperature, a slightly distorted monoclinic $P2_1/c$ symmetry for the crystal structure was found to fit the diffraction pattern better than the orthorhombic *Pnma* symmetry does. The simple ferromagnetic arrangement of the Mn spins

is consistent with the interaction being dominated by the DE interaction. Surprisingly, the diluted Ce spins become ordered at a relatively high temperature, showing that the coupling between the Mn and Ce spins is quite strong. We finally remark that the other rare earths in the related compounds were usually found [26–28] to be ordered at a lower temperature (below 30 K). Apparently, the magnetic coupling between the Mn 3d moments and the Ce 4f spins is stronger than between the Mn and other rare earths in the manganites.

Acknowledgment

References

[1] von Helmont R, Wecker J, Holzapfel B, Schultz L and Samwer K 1993 *Phys. Rev. Lett.* **71** 2331
[2] Jin S, Tiefel T H, McCormack M, Fastnacht R A, Ramesh R and Chen L H 1994 *Science* **264** 413
[3] Kuwarhara H, Tomioka Y, Asamitsu A, Moritomo Y and Tokura Y 1995 *Science* **270** 961
[4] Schiffer P, Ramirez A P, Bao W and Cheong S-W 1995 *Phys. Rev. Lett.* **75** 3336
[5] Coey J M, Viret M, Ramno L and Ounadjela K 1995 *Phys. Rev. Lett.* **75** 3910
[6] Asamitsu A, Moritomo Y, Tomioka Y, Arima T and Tokura Y 1995 *Nature* **373** 407
[7] Zener C 1951 *Phys. Rev.* **82** 403
[8] de Gennes P-G 1960 *Phys. Rev.* **118** 141
[9] Millis A J, Littlewood P B and Shraiman B I 1995 *Phys. Rev. Lett.* **74** 5144
[10] Hwang H Y, Cheong S-W, Radaelli P G, Marezio M and Batlogg B 1995 *Phys. Rev. Lett.* **75** 914
[11] For example see
    Rao C N R and Raveau B (ed) 1998 *Colossal Magnetoresistance, Charge Ordering and Related Properties of Manganese Oxides* (Singapore: World Scientific)
[12] Smolyaninova V N, Hamilton J J, Greene R L, Mukovskii Y M, Karabashev S G and Balbashov A M 1997 *Phys. Rev.* B **55** 5640
[13] Mandal P and Das S 1997 *Phys. Rev.* B **56** 15073
[14] Das S and Mandal P 1997 *Z. Phys.* B **104** 7
[15] Das S and Mandal P 1997 *Indian J. Phys.* A **71** 231
[16] Gebhardt J R, Roy S and Ali N 1999 *J. Appl. Phys.* **85** 5390
[17] Sundaresan A, Caignaert V, Maignan A, Raveau B and Suard E 1999 *Phys. Rev.* B **60** 533
[18] Huang Q, Santoro A, Lynn J W, Erwin R W, Borchers J A, Peng J L, Ghosh K and Greene R L 1998 *Phys. Rev.* B **58** 2684
[19] Lebedev O I, Van Tendeloo G, Amelinckx S, Leibold B and Habermeier H-U 1998 *Phys. Rev.* B **58** 8065
[20] Hervieu M, Van Tendeloo G, Caignaert V, Maignan A and Raveau B 1996 *Phys. Rev.* B **53** 14274
[21] Cox D E, Iglesias T, Shirane G, Hirota K and Endoh Y 1999 *Powder Diffract.* **14** 147
[22] Huang Q, Lynn J W, Erwin R W, Santoro A, Dender D C, Smolyaninova V N, Ghosh K and Greene R L 2000 *Phys. Rev.* B **61** 8895
[23] Lobanov M V, Balagurov A M, Pomjakushin V Ju, Fischer P, Gutmann M, Abakumov A M, D'yachenko O G, Antipov E V, Lebedev O I and Van Tendeloo G 2000 *Phys. Rev.* B **61** 8941
[24] Larson A C and Von Dreele R B 1990 General structure analysis system *Los Alamos National Laboratory Report* LA-UR-86-748
[25] Rietveld H M 1969 *J. Appl. Crystallogr.* **2** 65
[26] Millange F, Gaignaert V, Mather G, Suard E and Raveau B 1996 *J. Solid State Chem.* **127** 131
[27] Snyder G J, Booth C H, Bridges F, Hiskes R, Di Carolis S, Beasley M R and Geballe T H 1997 *Phys. Rev.* B **55** 6453
[28] Fauth F, Suard E, Martin C and Millange F 1998 *Physica* B **427** 241–3